Journal of
Materials Chemistry C

PAPER

View Article Online
View Journal

Cite this: DOI: 10.1039/c5tc03344f

Unexpected $SiMe_3$ effect on color-tunable and fluorescent probes of dendritic polyphenyl naphthalimides with aggregation-induced emission enhancement†

Hua Wang, Yan Liang, Huanling Xie, Haifeng Lu, Shigui Zhao* and Shengyu Feng*

Received 15th October 2015,
Accepted 15th December 2015

DOI: 10.1039/c5tc03344f

www.rsc.org/MaterialsC

In this paper, two new organic dyes derived from 1,8-naphthalimide and dendritic polyphenyl were designed and synthesized. Both the dyes exhibited unique aggregation-enhanced emission enhancement properties in methanol/water mixtures. The traditional fluorescent materials 1,8-naphthalimides were successfully transformed to AIE-active materials based on the dendritic polyphenyl structure. Furthermore, **NPI-Ph** and **NPI-Si** displayed excellent optical properties, such as solvent-induced emission changes from deep blue to light green, and the sensitive fluorescence response to nitroaromatic explosives. Interestingly, an unexpected $SiMe_3$ effect was found in the two dyes: the $SiMe_3$-containing compound **NPI-Si** exhibited remarkably enhanced optical properties compared with the non-$SiMe_3$ compound **NPI-Ph** such as a wider color-tunable range and higher sensitivity for the fluorescence detection of nitroaromatic explosives. The dendritic polyphenyl strategy and the $SiMe_3$ effect reported in this work will provide guidance to the design of AIE-active molecules and fluorescent materials for detecting nitroaromatic explosives.

Introduction

Dendritic polyphenyl derivatives, which contain benzene with multiple contiguous phenyl substituents, can be applied in various areas in science and technology, including materials for optoelectric devices,[1–3] template materials of supramolecular self-assembly,[4,5] and grapheme precursors.[6,7] In these compounds, aryl substituents are not constrained by the additional bonds in the aromatic core plane. Thus, aryl substituents exhibit large and twisted angles with the central benzene. These nonplanar topologies can hold conjugated molecules. Therefore, these compounds typically show greater gaps between the highest-occupied (HOMO) and lowest-unoccupied molecular orbitals (LUMO), lower degrees of self-association, less efficient packing, and higher solubility.[8,9]

In 2007, Tang *et al.* found that compounds with biphenyl derivatives exhibit aggregation-induced emission (AIE) properties.[10–12] The mechanism can be attributed to the phenyl restriction of intramolecular rotations. In our opinion, dendritic polyphenyl derivatives which have similar structures to biphenyl probably have AIE properties. Therefore, hexaphenylbenzene (**HPB**) was synthesized, and its optical properties were investigated to prove our thought in this work. The synthesis process and characterization were shown in the ESI.† It was exciting that **HPB** exhibited excellent aggregation-enhanced emission (AIEE) (Fig. S1, ESI†). According to the result, we believe that the **HPB** derivatives with propeller molecular structures may probably exhibit AIEE properties.

1,8-Naphthalimides (NPIs) are recently considered as important organic fluorophores and can be extensively applied in fluorescent sensors, optoelectronic materials, and imaging agents, among others.[13–19] However, the applications of NPIs are greatly limited because of the "aggregation-caused quenching" of fluorescence, which can be attributed to the tendency of charge-separated planar π surfaces of NPIs to cause π–π stacking interactions in the aggregated state.[20] Therefore, the feasibility of transforming NPIs to AIE-active molecules will be considered as great development. However, only a few NPI-based AIE-active molecules have been reported up to now.[21,22]

In this paper, two new NPI derivatives, namely, **NPI-Ph** and **NPI-Si**, with molecular structures similar to that of **HPB** were designed and synthesized (Scheme 1). It was exciting that both the dyes exhibited unique AIEE properties. The result was a good prove to our previous hypothesis: the dendritic polyphenyl structure was a successful strategy which transforms the traditional fluorescent materials to AIE-active materials. Furthermore, **NPI-Ph** and **NPI-Si** displayed excellent optical properties, such as solvent-induced emission changes from deep blue to light green,

School of Chemistry and Chemical Engineering, School of Material Science & Engineer, Key Laboratory of Special Functional Aggregated Materials & Key Laboratory of Colloid and Interface Chemistry (Shandong University), Ministry of Education, Shandong University, Jinan, 250100, People's Republic of China. E-mail: fsy@sdu.edu.cn; Fax: +86-531-88564464; Tel: +86-531-88364866

† Electronic supplementary information (ESI) available: The synthesis, characterization of HPB. See DOI: 10.1039/c5tc03344f

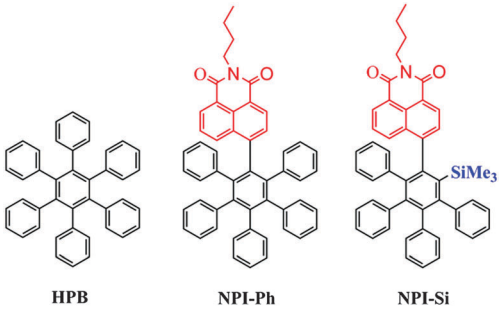

Scheme 1 Molecular structures of **HPB**, **NPI-Ph**, and **NPI-Si**.

and sensitive fluorescence response to nitroaromatic explosives. Interestingly, an unexpected $SiMe_3$ effect was found in the two dyes: the $SiMe_3$-containing compound **NPI-Si** exhibited remarkably enhanced optical properties compared with the non-$SiMe_3$ compound **NPI-Ph** such as a wider color-tunable range and higher sensitivity for the fluorescence detection of nitroaromatic explosives.

Experimental section

Material

4-Bromo-1,8-naphthalic anhydride, *n*-butylamine, phenylacetylene, $Pd(PPh_3)_2Cl_2$, PPh_3, CuI, triethylamine, and 2,3,4,5-tetraphenylcyclopenta-2,4-dienone were purchased from Aladdin Industrial Company. Ethynyltrimethylsilane was obtained from Beijing HWRK Chem. Co. LTD and used after fractionation (Scheme 2).

Synthesis of *N*-butyl-4-bromo-1,8-naphthalimide (2)

The synthesis was performed according to the published references. 4-Bromo-1,8-naphthalic anhydride (**1**) (1.38 g, 5 mmol) and *n*-butylamine (0.73 g, 10 mmol) were dissolved in 100 mL of ethanol. The reaction mixture was stirred and refluxed for 5 h. The crude product was obtained by filtration after the mixture was cooled to room temperature. The crude product was then purified by silica gel column chromatography using CH_2Cl_2/hexane (2 : 1, v/v) as an eluent to afford a white solid product. Yield: 1.22 g (70%).

^{1}H NMR ($CDCl_3$, 400 MHz, ppm): δ 8.67 (d, 1H), 8.60 (d, 1H), 8.58 (d, 1H), 8.07 (d, 1H), 7.85–7.89 (m, 1H), 4.19 (t, 2H), 1.70–1.78 (m, 2H), 1.44–1.55 (m, 2H), 1.00 (t, 3H). HRMS (FAB) calcd for $C_{16}H_{14}BrNO_2$ $[M + H]^+$ 332.0286, found 332.0027.

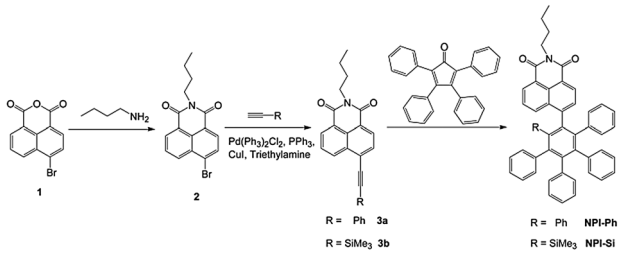

Scheme 2 The synthesis process of **NPI-Ph** and **NPI-Si**.

Synthesis of *N*-butyl-4-phenylacetylene-1,8-naphthalimide (3a)

The synthesis was conducted according to the published references. **2** (1.00 g, 3.00 mmol), phenylacetylene (0.306 g, 3.00 mmol), $Pd(PPh_3)_2Cl_2$ (112 mg, 0.16 mmol), PPh_3 (40 mg, 0.16 mmol), CuI (32 mg, 0.16 mmol), and 2 mL of triethylamine were added to anhydrous ethanol (50 mL). The reaction was stirred under reflux for 12 h under the argon atmosphere, cooled to room temperature, and then filtered to obtain the product. Subsequently, the crude product was purified by chromatography on silica gel using a hexane/EA (10 : 1) mixture as an eluent. A light yellow solid was then obtained. Yield: 0.66 g (55%).

^{1}H NMR ($CDCl_3$, 400 MHz, ppm): δ 8.66 (d, 1H), 8.59 (d, 1H), 8.57 (d, 1H), 7.98 (d, 1H), 7.86 (d, 1H), 7.70 (m, 1H), 7.46 (m, 1H), 4.21 (t, 2H), 1.73–1.79 (m, 2H), 1.44–1.53 (m, 2H), 0.99 (m, 3H). HRMS (FAB) calcd $C_{24}H_{19}NO_2$ for $[M + H]^+$ 354.1494, found 354.1273.

Synthesis of *N*-butyl-4-trimethylsilylethynyl-1,8-naphthalimide (3b)

The synthesis was performed according to the published references. **2** (1.00 g, 3.00 mmol), ethynyltrimethylsilane (0.306 g, 3.00 mmol), $Pd(PPh_3)_2Cl_2$ (112 mg, 0.16 mmol), PPh_3 (40 mg, 0.16 mmol), CuI (32 mg, 0.16 mmol), and 2 mL of triethylamine were added to anhydrous ethanol (50 mL). The reaction was stirred under reflux for 12 h under the argon atmosphere, cooled to room temperature, and then filtered to obtain the product. The crude product was then purified by chromatography on silica gel using a hexane/EA (10 : 1) mixture as an eluent. A light yellow solid was then obtained. Yield: 0.66 g (55%).

^{1}H NMR ($CDCl_3$, 400 MHz, ppm): δ 8.66 (d, 1H), 8.59 (d, 1H), 8.57 (d, 1H), 7.98 (d, 1H), 7.86 (d, 1H), 7.70 (m, 1H), 7.46 (m, 1H), 4.21 (t, 2H), 1.73–1.79 (m, 2H), 1.44–1.53 (m, 2H), 1.00 (m, 3H). HRMS (FAB) calcd $C_{21}H_{23}NO_2Si$ for $[M + H]^+$ 350.1576, found 350.1540.

Synthesis of *N*-butyl-4-pentaphenylbenzene-1,8-naphthalimide (NPI-Ph)

3a (0.5 g, 1.42 mmol) and 2,3,4,5-tetraphenylcyclopenta-2,4-dienone (0.54, 1.42 mmol) were added to 10 mL of diphenyl ether. The reaction was stirred under reflux for 30 h under the argon atmosphere and cooled to room temperature. The mixture was then poured into 200 mL of methanol to obtain the crude product. The crude product was purified by chromatography on silica gel using a hexane/EA (10 : 1) mixture as an eluent. A light yellow solid was then obtained. Yield: 0.63 g (62%).

^{1}H NMR (DMSO, 400 MHz, ppm): δ 8.33 (d, 1H), 8.25 (d, 1H), 8.08 (d, 1H), 7.77 (m, 1H), 7.66 (d, 1H), 6.98–7.00 (m, 5H), 6.76–6.93 (m, 14H), 6.62–6.69 (m, 4H), 6.52 (m, 2H), 3.91 (t, 2H), 1.50–1.54 (m, 2H), 1.26–1.32 (m, 2H), 0.88 (m, 3H). ^{13}C NMR ($CDCl_3$, 400 MHz, ppm): δ 164.31, 164.22, 146.07, 141.64, 140.80, 140.74, 140.20, 139.96, 139.66, 136.56, 133.41, 131.33, 131.29, 130.83, 130.70, 130.59, 130.14, 129.58, 127.45, 126.75, 126.70, 126.63, 126.61, 125.83, 125.75, 125.48, 122.33, 120.71, 40.22, 30.20, 20.42, 13.85. HRMS (FAB) calcd $C_{52}H_{39}NO_2$ for $[M + H]^+$ 710.3059, found 710.2901. Anal.calcd for $C_{52}H_{39}NO_2$: C 87.98%, H 5.54%, N 1.97%, O 4.51%; found: C 87.91%, H 5.63%, N 2.01%, O 4.42%.

Synthesis of *N*-butyl-4-trimethylsilyl-tetraphenylbenzene-1,8-naphthalimide (NPI-Si)

3b (0.5 g, 1.42 mmol) and 2,3,4,5-tetraphenylcyclopenta-2,4-dienone (0.54, 1.42 mmol) were added to 10 mL of diphenyl ether. The reaction was stirred under reflux for 30 h under the argon atmosphere and cooled to room temperature. The mixture was then poured into 200 mL of methanol to obtain the crude product. The crude product was purified by chromatography on silica gel using a hexane/EA (10 : 1) mixture as an eluent. A light yellow solid was then obtained. Yield: 0.63 g (62%).

^{1}H NMR (DMSO, 400 MHz, ppm): δ 8.42 (d, 1H), 8.33 (d, 1H), 8.22 (d, 1H), 7.88 (d, 1H), 7.82 (t, 1H), 7.03–7.24 (m, 7H), 6.69–6.91 (m, 12H), 6.53 (t, 1H), 6.45 (t, 1H), 3.99 (t, 2H), 1.58–1.61 (m, 2H), 1.31–1.37 (m, 2H), 0.90–0.94 (m, 3H), 0.01 (s, 1H). ^{13}C NMR ($CDCl_3$, 400 MHz, ppm): δ 143.35, 142.28, 141.67, 140.58, 140.21, 139.92, 139.44, 137.39, 134.02, 132.09, 132.01, 131.63, 131.31, 130.96, 130.89, 130.68, 130.55, 130.31, 129.62, 127.64, 126.93, 126.80, 126.65, 126.58, 126.55, 126.29, 126.20, 126.13, 125.97, 125.44, 125.27, 122.41, 121.48, 40.33, 30.24, 20.44, 13.86, 3.06. 29Si NMR ($CDCl_3$, 400 MHz, ppm): δ −4.26. HRMS (FAB) calcd $C_{49}H_{43}NO_2Si$ for $[M + H]^+$ 706.3141, found 706.3000. Anal. calcd for $C_{49}H_{43}NO_2Si$: C 83.37%, H 6.14%, N 1.98%, O 4.53%; found: C 83.40%, H 6.17%, N 1.99%, O 4.60%.

Results and discussion

Fig. 1 shows the UV-visible absorption and fluorescence emission spectra of **NPI-Ph** and **NPI-Si** in CH_2Cl_2 solution. The absorption bands for **NPI-Ph** were observed at 242, 346, and 363 nm, whereas those for **NPI-Si** were observed at 240, 345, and 363 nm. The fluorescence emission bands in CH_2Cl_2 solution for **NPI-Ph** and **NPI-Si** were observed at 416 and 427 nm at 298 K. And the fluorescence bands at 77 K for two dyes were 406 and 407 nm. The two compounds exhibited similar UV-visible absorptions and the fluorescence emission spectra in dilute CH_2Cl_2 solution.

The emission bands of **NPI-Ph** and **NPI-Si** showed a significant bathochromic shift when solvent polarity was increased (Fig. 2). Detailed data are provided in Table 1.

NPI-Ph displayed blue fluorescence (λ_{em} = 396 nm) in hexane and green emission (λ_{em} = 463 nm) in CH_3OH, and the shifts of these emissions were as large as 67 nm. Interestingly,

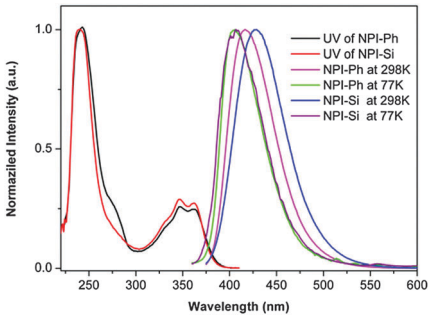

Fig. 1 UV-visible absorption spectra (left) and the fluorescence emission spectra (right, λ_{ex} = 360 nm) of **NPI-Ph** and **NPI-Si** in 10 μM CH_2Cl_2 solution.

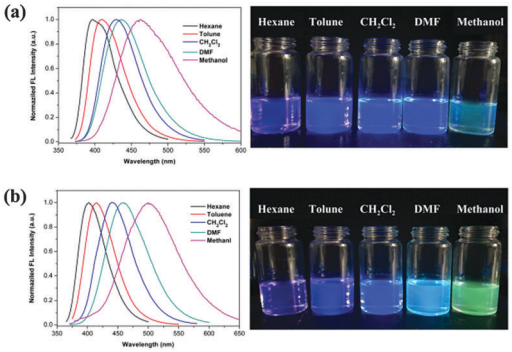

Fig. 2 (a) Normalized emissions of **NPI-Ph** (a) and **NPI-Si** (b) in different solvents and digital images of **NPI-Ph** in different solvents under UV irradiation at 365 nm.

Table 1 The fluorescence emission data of **NPI-Ph** and **NPI-Si** in different solvents

Compounds	Hexane λ_{em}/nm	Toluene λ_{em}/nm	CH_2Cl_2 λ_{em}/nm	DMF λ_{em}/nm	CH_3OH λ_{em}/nm
NPI-Ph	396	409	427	437	462
NPI-Si	401	415	441	458	500

these results were different from **NPI-Si**. The dye **NPI-Si** displayed blue fluorescence (λ_{em} = 401 nm) in hexane and green emission (λ_{em} = 500 nm) in CH_3OH, and the shifts of these emissions were as large as 103 nm. These large shifts in different solvents demonstrate that the two dyes show a solvatochromic effect. However, the effects of the polarities of the solvents on the two dyes were quite different. **NPI-Si** exhibited a wider color-tunable range than **NPI-Ph**. NPIs were the electron acceptors in the two dyes. Contrary to **NPI-Ph**, **NPI-Si** showed an asymmetrical molecular structure. Moreover, "dπ–pπ" existed between the Si and benzene ring which reduced the electron density of the center phenyl ring and enhanced the molecular polarity. Therefore, **NPI-Si** showed larger molecular polarity than **NPI-Ph**, which resulted in more remarkable solvent-induced emission changes.

The large shifts in the different solvents and at different temperatures demonstrate that the two dyes show twisted intramolecular charge transfer (TICT) activities.[22] The fluorescence intensities of **NPI-Ph** and **NPI-Si** decreased when the solvent polarity increased. Interestingly, the emission intensity of **NPI-Ph** and **NPI-Si** dramatically increased when the H_2O fraction of 50% (v/v%) was added into the CH_3OH solution (Fig. 3). This phenomenon is a characteristic of AIEE.

The AIEE process was directly investigated by plotting the graph of emission area *versus* different H_2O fractions in CH_3OH, and a clear trend was observed. According to the Tang's report, the restriction of intramolecular rotation was inferred to be the primary factor of the AIEE effect.[10–12] The TICT feature dominated the emission intensity of **NPI-Ph** and that of **NPI-Si** decreased at small fractions of H_2O. By contrast, **NPI-Ph** and **NPI-Si** aggregated in CH_3OH mixed solvents with the 50% H_2O fraction, and the emission intensity quickly increased. However, emission intensity began to decrease when the H_2O fraction exceeded 50%.

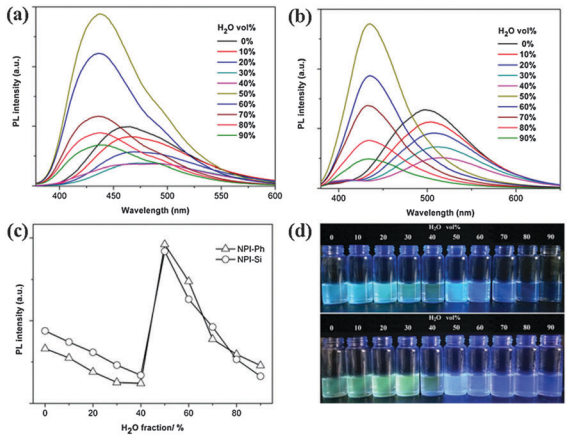

Fig. 3 Fluorescence spectra of **NPI-Ph** (a) and **NPI-Si** (b) in the $CH_3OH–H_2O$ mixture with different H_2O fractions. (c) Plots of fluorescent areas of **NPI-Ph** and **NPI-Si** *versus* the water fraction in the $CH_3OH–H_2O$ mixture (d) digital images of **NPI-Ph** and **NPI-Si** with different H_2O fractions under UV irradiation at 365 nm.

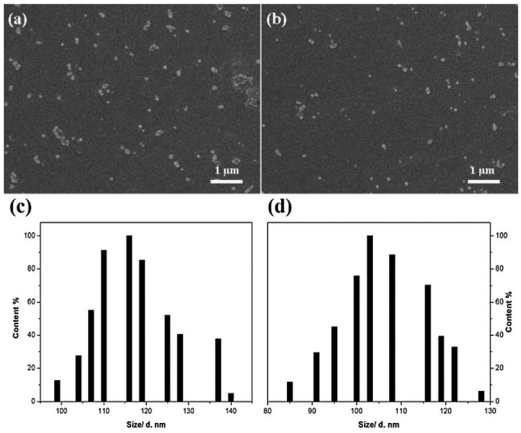

Fig. 4 The SEM pictures of **NPI-Ph** (a) and **NPI-Si** (b) aggregates in $CH_3OH–H_2O$ (H_2O fraction: 50%); the DLS spectra of **NPI-Ph** (c) and **NPI-Si** (d) aggregates in $CH_3OH–H_2O$ (H_2O fraction: 50%).

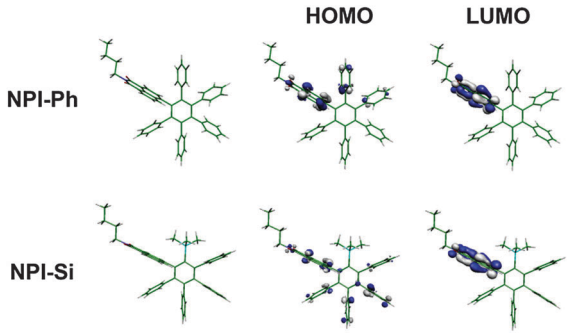

Fig. 5 Frontier-molecular-orbitals of the density functional theory-optimized ground state structures of **NPI-Ph** and **NPI-Si**.

This phenomenon can also be attributed to TICT. The variation of fluorescence intensity exhibited a unique "Z" shape when the H_2O fraction was increased from 0% to 90%. The absorptions of **NPI-Ph** and **NPI-Si** in H_2O fractions of 0%, 50%, and 90% are illustrated in Fig. S2 (ESI†). The absorption spectra of the two dyes at the 50% H_2O fraction show bands that differ from those at H_2O fractions of 0% and 90%. Therefore, the **NPI-Ph** and **NPI-Si** molecules have different packing aggregation states which lead to AEE. In addition, the aggregate of **NPI-Si** in H_2O was stable for about two months, whereas that of **NPI-Ph** subsided after three days. Therefore, **NPI-Si** can be well used in water or other mixed solvents with strong fluorescence.

The scanning electron microscope (SEM) and dynamic light scattering (DLS) were proceeded to further confirm the formation of molecular (**NPI-Ph** and **NPI-Si**) aggregation. From the SEM pictures in Fig. 4(a) and (b), it could be clearly seen that the molecular aggregates were formed when water was added. As revealed by DLS analysis, the average particle diameter becomes larger with the increase of the H_2O fraction. The tendency was same to Tang's reports.[11,12] The average particle diameters for **NPI-Ph** were 93 nm, 119 nm and 153 nm, whereas those for **NPI-Si** were 78 nm, 102 nm and 139 nm in the $H_2O–CH_3OH$ (H_2O fraction: 40%, 50% and 60%) mixture, respectively.

The structures of **NPI-Ph** and **NPI-Si** in the gas phase were optimized at the B3LYP/6-31G* levels. The frontier-molecular-orbitals (FMOs) of **NPI-Ph** and **NPI-Si** were concentrated on the NPI moiety rather than on the phenyl substituent (Fig. 5). Hence, their photophysical characteristics, *i.e.*, spectral absorption and emission regions, were expected to be similar and dominated by the NPI unit. The phenyl groups moderately contributed to the HOMO levels but did not contribute to the LUMOs. This characteristic can be considered as a signature of a weak electron donor. The energy levels of the HOMO and LUMO for **NPI-Ph** were −6.09 and −2.25 eV, respectively, whereas the corresponding values for **NPI-Si** were −6.08 and −2.28 eV. The energy gaps for **NPI-Ph** and **NPI-Si** were 3.84 and 3.80 eV, respectively. This finding indicates that the two dyes have similar FMOs and energy gaps, which resulted in the similar absorption and emission spectra in dilute solution.

In recent days, the development of highly sensitive fluorescent sensor materials for the detection of explosives at low concentration is still a challenge.[23,24] The fluorescent AIE-active materials have been proved to be the fantastic selection for fluorescence detection.[25,26] Thus, **NPI-Ph** and **NPI-Si** with excellent fluorescence properties are expected to work as excellent fluorescent sensors for detecting electron-deficient quenchers, such as nitroaromatic explosives.[27,28] In this work, we used picric acid (PA) as a model explosive. The quenching processes of the PL of the dyes were investigated by monitoring the changes in their PL in response to PA addition.

The PL intensities of the **NPI-Ph** and **NPI-Si** were both progressively weakened when an increasing amount of PA was added into the solution with nanoaggregates in the mixture solvents. The fluorescence spectra in Fig. 6 show that virtually no light was emitted from the nanoaggregates in the 50% aqueous mixture when the PA concentration was increased to 60 μM.

The Stern–Volmer plot of relative PL intensity (I_0/I) *versus* PA concentration in the aqueous mixtures with the 50 vol% H_2O content shows a curve bending upward, instead of a linear

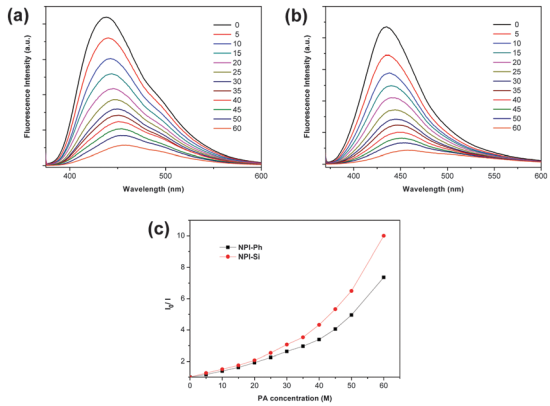

Fig. 6 Changes in the PL spectra of **NPI-Ph** (a) and **NPI-Si** (b) with the addition of different amounts of PA in the THF–water mixture (5 : 5 v/v); λ_{ex} = 322 nm; c = 5 μM. (c) Stern–Volmer plots of I_0/I *versus* [PA] in THF–water mixtures with f_w of 50 vol%.

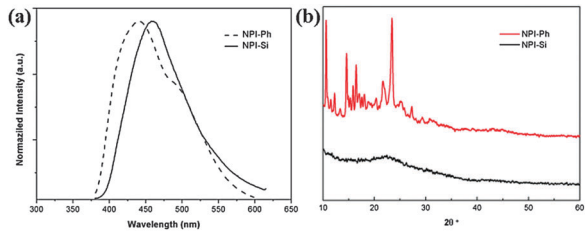

Fig. 7 (a) The fluorescence emission spectra of **NPI-Ph** and **NPI-Si** in the solid state; (b) the XRD spectra of **NPI-Ph** and **NPI-Si** solid powder.

relationship (Fig. 6). This finding indicates that the two dyes have a superamplification effect in the detection of nitroaromatic explosives.[25] PL annihilation caused by static quenching or simultaneous dynamic and static quenching possibly led the **NPI-Ph** and **NPI-Si** luminogens to produce nonlinear Stern–Volmer plots. Therefore, **NPI-Ph** and **NPI-Si** were both highly sensitive chemosensors for explosive detection. Moreover, the silicon-containing dye **NPI-Si** was much more sensitive for explosive detection than **NPI-Ph**. This phenomenon can also be attributed to the greater molecular polarity of **NPI-Si** than **NPI-Ph**.

The solid state fluorescence of two dyes, **NPI-Ph** and **NPI-Si** was measured and investigated. As shown in Fig. 7(a), the fluorescence emission bands in the solid state for **NPI-Ph** and **NPI-Si** were observed at 442 nm and 459 nm. In the solid state, **NPI-Si** also exhibited a slight red shift than **NPI-Ph** which was similar to that in solution. In the XRD spectra of two dyes in solid powder (Fig. 7b), it could be clearly seen that **NPI-Ph** displayed several peaks when **NPI-Si** nearly have no peaks. It indicated that the packing of **NPI-Si** molecules was amorphous in solid powder while **NPI-Ph** molecules were ordered in some degree. According to the reports, the reason could be attributed to the asymmetrical molecular structure of **NPI-Si** and $SiMe_3$ group unique effects.[29,30]

Conclusions

In summary, two novel dyes derived from 1,8-naphthalimide and dendritic polyphenylene were designed and synthesized in this work. The two dyes showed unique AIEE characteristics. Therefore, the dendritic polyphenyl structure was a successful strategy which transforms the traditional fluorescent materials to AIE-active materials. Furthermore, **NPI-Ph** and **NPI-Si** displayed excellent optical properties, such as solvent-induced emission changes from deep blue to light green, and the sensitive fluorescence response to nitroaromatic explosives. Interestingly, an unexpected $SiMe_3$ effect was found in the two dyes: the $SiMe_3$-containing compound **NPI-Si** exhibited remarkably enhanced optical properties compared with the non-$SiMe_3$ compound **NPI-Ph** such as a wider color-tunable range and higher sensitivity for the fluorescence detection of nitroaromatic explosives. The dendritic polyphenyl strategy and the $SiMe_3$ effect reported in this work will provide guidance to the molecular structural design for detecting nitroaromatic explosives.

Acknowledgements

This work was financially supported by the Shandong special fund for independent innovation and achievements transformation (No. 2014ZZCX01101), the National Natural Science Foundation of China (No. 21274080) and the China Postdoctoral Science Foundation (No. 2015M580590).

Notes and references

1 A. Pogantsch, F. P. Wenzl, E. J. List, G. Leising, A. C. Grimsdale and K. Müllen, *Adv. Mater.*, 2002, **14**, 1061–1064.
2 X. Sun, X. Xu, W. Qiu, G. Yu, H. Zhang, X. Gao, S. Chen, Y. Song and Y. Liu, *J. Mater. Chem.*, 2008, **18**, 2709–2715.
3 K. J. Thomas, M. Velusamy, J. T. Lin, S.-S. Sun, Y.-T. Tao and C.-H. Chuen, *Chem. Commun.*, 2004, 2328–2329.
4 M. Hoffmann, J. Kärnbratt, M. H. Chang, L. M. Herz, B. Albinsson and H. L. Anderson, *Angew. Chem.*, 2008, **120**, 5071–5074.
5 M. Alam, Y. S. Kim, S. Ogawa, A. Tsuda, N. Ishii and T. Aida, *Angew. Chem.*, 2008, **120**, 2100–2103.
6 A. Narita, X. Feng, Y. Hernandez, S. A. Jensen, M. Bonn, H. Yang, I. A. Verzhbitskiy, C. Casiraghi, M. R. Hansen and A. H. Koch, *Nat. Chem.*, 2014, **6**, 126–132.
7 L. Dössel, L. Gherghel, X. Feng and K. Müllen, *Angew. Chem., Int. Ed.*, 2011, **50**, 2540–2543.
8 E. Gagnon, T. Maris, P.-M. Arseneault, K. E. Maly and J. D. Wuest, *Cryst. Growth Des.*, 2009, **10**, 648–657.
9 U. Kumar and T. X. Neenan, *Macromolecules*, 1995, **28**, 124–130.
10 K. Cathy and B. Zhongá Tang, *Chem. Commun.*, 2007, 70–72.
11 Y. Hong, J. W. Lam and B. Z. Tang, *Chem. Soc. Rev.*, 2011, **40**, 5361–5388.
12 Y. Hong, J. W. Lam and B. Z. Tang, *Chem. Commun.*, 2009, 4332–4353.
13 M. H. Lee, J. Y. Kim, J. H. Han, S. Bhuniya, J. L. Sessler, C. Kang and J. S. Kim, *J. Am. Chem. Soc.*, 2012, **134**, 12668–12674.
14 M. Kumar, N. Kumar and V. Bhalla, *Chem. Commun.*, 2013, **49**, 877–879.

15 R. M. Duke, E. B. Veale, F. M. Pfeffer, P. E. Kruger and T. Gunnlaugsson, *Chem. Soc. Rev.*, 2010, **39**, 3936–3953.
16 S. Mukherjee and P. Thilagar, *Chem. – Eur. J.*, 2014, **20**, 8012–8023.
17 P. Gopikrishna, D. Das and P. K. Iyer, *J. Mater. Chem. C*, 2015, **3**, 9318–9326.
18 S. Luo, J. Lin, J. Zhou, Y. Wang, X. Liu, Y. Huang, Z. Lu and C. Hu, *J. Mater. Chem. C*, 2015, **3**, 5259–5267.
19 F. Grepioni, S. d'Agostino, D. Braga, A. Bertocco, L. Catalano and B. Ventura, *J. Mater. Chem. C*, 2015, **3**, 9425–9434.
20 C. Han, T. Huang, Q. Liu, H. Xu, Y. Zhuang, J. Li, J. Hu, A. Wang and K. Xu, *J. Mater. Chem. C*, 2014, **2**, 9077–9082.
21 S. Mukherjee and P. Thilagar, *Chem. Commun.*, 2013, **49**, 7292–7294.
22 Y. Li, Y. Wu, J. Chang, M. Chen, R. Liu and F. Li, *Chem. Commun.*, 2013, **49**, 11335–11337.
23 W. Xue, Y. Zhang, J. Duan, D. Liu, Y. Ma, N. Shi, S. Chen, L. Xie, Y. Qian and W. Huang, *J. Mater. Chem. C*, 2015, **3**, 8193–8199.
24 Z. Ding, Q. Zhao, R. Xing, X. Wang, J. Ding, L. Wang and Y. Han, *J. Mater. Chem. C*, 2013, **1**, 786–792.
25 J. Liu, Y. Zhong, P. Lu, Y. Hong, J. W. Lam, M. Faisal, Y. Yu, K. S. Wong and B. Z. Tang, *Polym. Chem.*, 2010, **1**, 426–429.
26 S. Kaur, A. Gupta, V. Bhalla and M. Kumar, *J. Mater. Chem. C*, 2014, **2**, 7356–7363.
27 J. C. Sanchez, A. G. DiPasquale, A. L. Rheingold and W. C. Trogler, *Chem. Mater.*, 2007, **19**, 6459–6470.
28 H. Sohn, M. J. Sailor, D. Magde and W. C. Trogler, *J. Am. Chem. Soc.*, 2003, **125**, 3821–3830.
29 E. Q. Procopio, M. Mauro, M. Panigati, D. Donghi, P. Mercandelli, A. Sironi, G. D'ALFONSO and L. De Cola, *J. Am. Chem. Soc.*, 2010, **132**, 14397–14399.
30 H. Wang, Y. Liang, H. Xie, L. Feng, H. Lu and S. Feng, *J. Mater. Chem. C*, 2014, **2**, 5601–5606.

